Quasiclassical dynamics and kinetics of the N + NO → N_2 + O, NO + N atmospheric reactions

Pablo Gamallo,[a] Rodrigo Martínez,[b] R. Sayós,[a,*] and Miguel González[a,*]

[a]Departament de Química Física i IQTC, Universitat de Barcelona, C/ Martí i Franquès 1, 08028 Barcelona (Spain)

[b]Departamento de Química, Universidad de La Rioja, C/ Madre de Dios, 51, 26006 Logroño (Spain)

Abstract

The kinetics and dynamics of the title reactions was studied, using the quasiclassical trajectory (QCT) method and two *ab initio* analytical potential energy surfaces (PESs) developed by our group. In addition to the rate constant (*T*: 10-5000 K), we also considered a broad set of dynamic properties as a function of collision energy (up to 1.0 eV) and the rovibrational state of NO(*v*=0-2,*j*=1,8,12). The production of N_2 + O, reaction (1), dominates the reactivity of the N + NO system over the conditions studied, as expected from the large energy barriers associated to the NO + N exchange reaction, reaction (2). Moreover, the ground PES, which is barrierless for reaction (1), plays a dominant role. Most of the results were interpreted according to the properties of the PESs involved and the kinematics of the system. The QCT rate constants of reaction (1) are in agreement with the experimental data (*T*: 47-3500 K), including very recent low temperature measurements, and also with variational transition state kinetics and most of quantum dynamics calculations. In addition, the QCT average vibrational energy content of the N_2 product also agrees with the experimental and quantum data. The PESs used here could also be useful to determine equilibrium and non-equilibrium reaction rates at very high temperatures (e.g., 5000-15000 K).

Keywords: N + NO, N_2 + O reaction, NO + N exchange reaction, kinetics, dynamics, theoretical study, quasiclassical trajectory method

Tables: 3 **Figures:** 10 **Proofs to**: Prof. Miguel González

* Corresponding authors: r.sayos@ub.edu and miguel.gonzalez@ub.edu

I. Introduction

The reaction of atomic nitrogen with nitric oxide has been the subject of numerous studies in the last decade. In this system two reactive processes can occur. The first one involves the production of molecular nitrogen via the highly exothermic reaction channel,[1]

$$N(^4S) + NO(X^2\Pi) \rightarrow N_2(X^1\Sigma_g^+) + O(^3P) \qquad \Delta_r H^\circ_{0\,K} = -3.178 \text{ eV}, \qquad (1)$$

while the second one involves the exchange of the nitrogen atom in the nitric oxide molecule,

$$N(^4S) + N'O(X^2\Pi) \rightarrow NO(X^2\Pi) + N'(^4S) \qquad \Delta_r H^\circ_{0\,K} = 0 \text{ eV}. \qquad (2)$$

Reaction (1) has been used to determine NO concentrations in low-pressure discharge-flow systems and to measure NO concentrations in combustion exhaust gases. In addition to its practical implications, this reaction affects the stratosphere, since it acts as a sink for NO molecules[2,3]. The extinction of NO molecules prevents their introduction into the catalytic cycle of ozone depletion, where a single NO molecule destroys several O_3 molecules, which are vital to all forms of life on Earth.

The $N + NO \rightarrow N_2 + O$ reaction is also interesting from a theoretical perspective, as it proceeds via two potential energy surfaces (PESs).[4] The most important of them is the barrierless ground state PES ($^3A''$ surface), where the reaction proceeds without surmounting any energy barrier along the minimum energy path (MEP) connecting reactants and products. The other potential energy surface of interest is the first excited state PES ($^3A'$ surface), which has an early barrier of 0.36 eV and only contributes significantly to the reactivity of the system at high temperatures.[4] Moreover, as this relevant system involves a small number of atoms, a strong interaction between theory and experiment is expected.

Differing from the first reaction, reaction (2) presents a very low reactivity, due to the presence of a high energy barrier (>1 eV) on both the $^3A''$ and $^3A'$ PESs, which connects the two equivalent [N-O-N] minima involved in the N-atom exchange process.[4] The determination of the rate constant for this reaction is, however, of interest, and such data are very scarce and difficult to

obtain experimentally. Measurements on reaction (2) are reported in two isotopic studies,[5,6] but only at very high collision energies, while the present study focuses on thermal conditions and low-moderate collision energies.

Since the earlier theoretical works on the dynamics and kinetics of reaction (1) (see, e.g., Refs. 7, 8, 9, and 10), several theoretical methods have been applied to this system in order to better characterize its dynamics and kinetics properties, using *ab initio* based analytical PESs.[4] They include variational transition state theory (VTST)[4] and time-dependent real wave-packet (RWP)[11,12] approaches. These theoretical studies on reaction (1) show good agreement for the ground state PES, ^{3}A'', whereas the rate constants obtained with the VTST method are a factor of three larger than those obtained with RWPs for the excited state PES, ^{3}A'.

Here we employ the *ab initio* analytical representations of the ground and first excited PESs developed in our group,[4] to perform a theoretical study of the dynamics and kinetics of reactions (1) and (2), using the quasiclassical trajectory (QCT) method. The paper is organized as follows: Section II provides the computational details, Section III presents the QCT results (scalar and vector properties and microscopic reaction mechanisms) and the comparison with previous theoretical and experimental data. Finally, Section IV gives the summary and conclusions.

II. Computational method

The analytical representations (many-body expansion functions[13]) of the 1^3A'' and 1^3A' PESs used in this study (^{3}A'' and ^{3}A' PESs hereafter) were reported in Ref. 4. They are based on an *ab initio* CASSCF (10,9) study,[14] in which the standard correlation-consistent cc-pVTZ basis set was used. The dynamic correlation was treated using the CASPT2 method with the G2 correction to the Fock matrix.[14] Reaction (1) is barrierless on the ground (1^3A'') PES and has a barrier on the excited (1^3A') PES (N-atom abstraction through a saddle point of bent geometry), while reaction (2)

shows a large energy barrier on both potential energy surfaces (O-atom abstraction *via* a C_{2v} minimum).

Here, we investigated the dynamics of reaction (1) on the two PESs, as a function of collision energy (E_T), and the rovibrational level (v, j) of NO, using the QCT method.[15,16,17,18] The influence of temperature (T: 10-5000 K) on the dynamics and kinetics of reactions (1) and (2) has also been examined, using the same approach.

Although the QCT method was established long ago, it is still one of the most useful theoretical tools for studying chemical reaction dynamics. We verified the accuracy of the numerical integration of Hamilton's differential equations by analyzing the conservation of total energy and total angular momentum for each trajectory. The integration step size chosen (0.5×10^{-16} s) was found to fulfill the conservation requirements for all trajectories. The trajectories were started at an initial distance of 12 Å between the N atom and the center of mass of the NO molecule, thus ensuring that the interaction energy was negligible with respect to the available energy.

From some QCT check calculations it came out that for the main goal of this contribution, essentially centered in the study of reactivity and without paying attention to the rotational state distributions of the N_2, it was not necessary to account for the nuclear spin statistics due the homonuclear character of the N_2 product molecule. A RWP-J shifting investigation of the rotational distributions of N_2, taking into account the permutation symmetry and nuclear-spin statistics was reported in Ref. 12.

The dynamics of reaction (1) (the main process considered here), as a function of (E_T, v, j), has been studied with the NO molecule in the (v=0-2, j=1,8,12) rovibrational levels and within the 0-0.8 eV and 0.4-1.0 eV E_T intervals for the $1^3A''$ and $1^3A'$ PESs, respectively. In the dynamics study of reactions (1) and (2) in the 10-5000 K T interval, the initial conditions (E_T, v, j) were sampled for each selected temperature [i.e., E_T and (v, j) from a Maxwell and a Boltzmann distribution, respectively].

For each initial condition (E_T, v, j) batches of 1×10^4 and 5×10^5 trajectories were calculated on the ground and excited PESs, respectively. At a given T, batches of 3×10^5 trajectories were calculated to determine cross sections, product state distributions and vector properties on the ^{3}A'' surface. As reactivity of the ^{3}A' surface was generally much lower than that of the ^{3}A'' PES, a larger number of trajectories was sampled in this case (9×10^6 at 1000 K, while 4×10^5 were sufficient at 5000 K). For reaction (1) the standard deviation of the cross sections at all temperatures studied was less than 1 % on both PESs, while for reaction (2) it varied from 17 % [ground PES (T=3000 K) and excited PES (T=2000 K)] to less than 5 % at 5000 K for both PESs. The standard deviation of reaction (1) distributions was maintained below 5 % in both PESs, whereas for reaction (2) distributions with a standard deviation below 5 % were recorded above 3000 K. Moreover, some additional calculations between 10 and 100 K were also performed on the ground PES, calculating, typically, 5×10^4 trajectories at each selected T.

III. Results and discussion

A. Rate constants

Figure 1 shows the dependence of the rate constant of reaction (1), k_1, on temperature for the ^{3}A'' and ^{3}A' PESs and for the sum of both contributions, $k_1 = k_1(^3\text{A''}) + k_1(^3\text{A'})$. In addition, Tables I and II show the QCT results obtained together with VTST[4] and quantum RWP J-shifting[12] results and experimental data[19,20,21,22,23,] on this reaction. The theoretical rate constant values reported were calculated on each PES and the results were multiplied by the electronic term in Equation (3), which accounts for the weight of each PES as a function of temperature:

$$\frac{3}{4\left(2 + 2\exp\left(\frac{-172.4}{T}\right)\right)} \qquad (3)$$

From 100 to 600 K the ^{3}A'' QCT rate constant of reaction (1) decreases with T and then increases monotonically with T, although the variation of $k_1(^3A'')$ with T is small. Thus, within the T: 100-600 K interval the rate constant changes from 3.38×10^{-11} to 2.34×10^{-11} cm^3 s^{-1} and at the highest temperature considered (T=5000 K) it has a value of 4.05×10^{-11} cm^3 s^{-1}. This small variation of $k_1(^3A'')$ over a very wide temperature range (T: 100-5000 K) is determined by the barrierless nature of the ground surface.[4] At the lowest temperature range explored $k_1(^3A'')$ increases with T (from 2.35×10^{-11} cm^3 s^{-1} at 10 K to 3.38×10^{-11} cm^3 s^{-1} at 100 K). In the case of the ^{3}A' PES, the rate constant of reaction (1) increases with temperature and varies by more than two orders of magnitude (8.60×10^{-14} to 1.10×10^{-11} cm^3 s^{-1}) in the 1000-5000 K temperature range. This considerable variation in the values of $k_1(^3A')$ is caused by the energy barrier on the excited surface.[4] There is no contribution of the excited surface to reactivity in the moderate and low T regions.

In general, $k_1(^3A'')$ is higher or much higher than $k_1(^3A')$ and the production of N_2 + O from N + NO [reaction (1)] arises, essentially, from the ground PES until 1500 K. From this temperature the sum $k_1(^3A'') + k_1(^3A')$ begins to deviate from $k_1(^3A'')$. At 1500, 2000, 3000, 4000 and 5000 K the $k_1(^3A'')/k_1(^3A')$ ratio is equal to 49.9, 20.7, 8.2, 5.1 and 3.7 respectively. Consequently, the ^{3}A'' barrierless PES is clearly predominant in the contribution to the rate constant of reaction (1), due to the energy barrier of the ^{3}A' PES.

For reaction (1), the QCT results show in general a good agreement with the VTST (ICVT/μOMT-SO)[12] results. In the case of the excited PES, this agreement is almost quantitative. The better QCT-VTST agreement found for the excited PES could be expected as this surface, unlike the barrierless ground PES, has an energy barrier along the MEP (0.379 eV; ZPE included).[4] In addition, the QCT calculations are in agreement with the experimental data over the entire temperature range, taking into account the error margins. Comparison with the quantum RWP J-shifting data[12] shows that the ^{3}A" QCT and RWP results are similar, but significant differences

appear in the ^{3}A' results. The RWP J-shifting $k_1(^3A')$ data were analyzed in Ref. 12, but the origin of the low values found remained unclear.

Figure 2 shows the dependence of the rate constant of reaction (2), k_2, on temperature for the ^{3}A'' and ^{3}A' PESs and for the sum of both contributions, $k_2 = k_2(^3A'') + k_2(^3A')$. Moreover, Table III shows the QCT results obtained together with the VTST data[4] for this reaction.

For both the ground and excited PESs, the QCT rate constant of reaction (2) increases monotonically with temperature and has very low values except for the higher temperatures studied. These results are expected as both surfaces have a large energy barrier for the N-atom exchange reaction.[4] The variation of $k_2(^3A'')$ and $k_2(^3A')$ with T is quite large and, in general, $k_2(^3A")$ is quite lower than $k_2(^3A')$, as the ^{3}A" surface has a larger energy barrier for exchange than the ^{3}A' surface (1.735 and 1.190 eV above reactants, including the ZPE, respectively).[4] For reaction (2), the QCT results are in quite good agreement with the VTST (ICVT/μOMT-SO)[12] results, which were obtained using the steady-state approximation.

State-specific rate constants for N + NO → N_2(v') + O and N + N'O → NO(v') + N' and reaction dynamics properties for thermal N + NO collisions are presented in the supplementary material of Ref. 24.

B. Cross sections

The dependence of the cross section of reaction (1), σ_1, as a function E_T for selected values of v, and j, NO(v=0,j=1,8,12), on the ground (^{3}A'') and excited (^{3}A') PESs, is shown in Figure 3. The results obtained for the other vibrational levels of NO explored (v=1,2) are similar. This also applies to the N + NO(v=0-2,j=1,8,12) → N_2(v') + O state-to-state cross sections, with the exception of reaction conditions close to the energy threshold for production of highly excited vibrational N_2. The cross sections for N + NO(v=1,2,j=1,8,12) → N_2 + O and the state-to-state cross sections for N + NO(v=0-2,j=1,8,12) → N_2(v') + O can be found in Ref. 24. The cross section

values reported, which are taken from the present QCT data and the RWP J-shifting data from Ref. 12, were calculated on each PES and the results were multiplied by the electronic term in Equation (3). Under the reaction conditions explored, reaction (2) has not been detected.

The cross section of reaction (1) on the ground PES, $\sigma_1(^3A'')$, strongly decreases with E_T in the 0-0.05 eV range ($\Delta\sigma/\Delta E_T \approx -5.60\times10^2$ Å^2 eV^{-1}). At higher E_T values this decrease becomes progressively less intense until the cross section is almost independent of E_T above 0.4 eV. This behavior is expected for a reaction taking place on a barrierless PES, as it is the case of the $^3A''$ surface. On the other hand, $\sigma_1(^3A'')$ presents a small dependence with the vibrational and rotational levels of the NO molecule. These results can be understood taking into account the absence of barrier and the high exoergicity of the main reaction on the ground surface.

The cross section of reaction (1) on the excited PES, $\sigma_1(^3A')$, increases with E_T within the collision energy range explored (0.4-1.0 eV; $\Delta\sigma/\Delta E_T \approx 2.25$ Å^2 eV^{-1}). This behavior is expected for a reaction taking place on a PES with an energy barrier for the reaction to be produced, as it occurs in the $^3A'$ surface. The plateau and further decrease of the cross section observed in the σ vs E_T dependence for this type of systems is not observed here because energies are not large enough to make it evident. We also observe here that, as in the case of the cross section for the ground surface, $\sigma_1(^3A')$ presents a small dependence with the vibrational and rotational levels of the NO molecule. These results can be rationalized taking into account that the $^3A'$ surface has an early barrier resulting from the high exoergicity of reaction (1) (Hammond's postulate), and in this situation it is well known (Polanyi's rules) that relative translational energy of reactants is particularly efficient to allow the system to evolve into products.

For the $^3A''$ surface, the decrease of σ with E_T mainly results from the b^2_{max} decrease with E_T, as the averaged reaction probability is almost constant (≈0.25) up to 0.4 eV and reaches a value of 0.34 at 0.8 eV [σ(QCT) = $\pi\, b^2_{max}\langle P_r\rangle$, where b_{max} and $\langle P_r\rangle$ are the maximum impact parameter and the reaction probability averaged over the range of impact parameters, respectively ($\langle P_r\rangle = N_r/N$;

number of reactive trajectories obtained divided by the number of trajectories calculated)]. In the case of the ^{3}A' surface the situation is different, as both b^2_{max} and $<P_r>$ increase with E_T.

From the cross section values it can be concluded that the ^{3}A'' PES plays a dominant role in the cross section of reaction (1), while the contribution of the ^{3}A' PES to this cross section is negligible at collision energies below 0.4 eV approx., due to the presence of an energy barrier. The dominant character of the ground PES was already evident in the rate constant analysis (cf. Section A).

C. Product state distributions

Figure 4 shows the average fractions of energy in products [$<f_i'>$, i=V (vibration), R (rotation), and T (translation)] for reaction (1) on the ground and excited potential energy surfaces as a function of collision energy and the rovibrational state of NO(v=0,j=1,8,12). As abovementioned in the case of the cross sections, the results are similar for the other v and j, reaction conditions studied. For the ^{3}A'' PES, $<f_T'>$ is almost independent of E_T (approx. 0.60), $<f_V'>$ is around 0.20-0.25, and $<f_R'>$ is about 0.10-0.20. The augment of rotational energy in products as collision energy increases is associated to the decrement of products vibrational energy with E_T. The role played by $<f_T'>$ and $<f_V'>$ in the case of the ^{3}A'' PES is reversed for the ^{3}A' PES. Therefore, when E_T increases $<f_T'>$ increases (0.35 to 0.38), $<f_V'>$ decreases (0.56 to 0.50), and $<f_R'>$ increases (0.09 to 0.12). There is a small dependence of the energy fractions with respect to the (v,j) state of NO, this being particularly evident for the excited PES.

The exothermicity of the reaction plays an important role in the energy distribution in products, releasing an important fraction of the available energy as internal energy of the N_2 molecule. Overall, approx. 40% (^{3}A'') and 65% (^{3}A') of the available energy is released as internal energy of N_2. The larger vibrational excitation resulting from the excited PES could be understood taking into account that it corresponds to an early barrier PES and, due to this fact, translational

energy of reactants is transformed into vibrational energy of products in a particularly efficient way.

For the overall reaction (^{3}A''+^{3}A' surfaces) in the wide temperature interval explored the majority of the available energy is channeled into relative translational energy of products (0.52-0.63), although a considerable energy fraction is also released as rovibrational energy of N_2 (0.48-0.38); see also Ref.24. The vibrational fraction increases slightly with temperature, from 0.25 at 100 K to 0.28 at 5000 K. This QCT value agrees with the experimental value reported in Ref. 25 (0.25) and with the previous quantum RWP *J*-shifting result (0.24).[12] The total average fractions of energy have been calculated according to the following expression:

$$\langle f'_i \rangle = \frac{\sigma(^3A'') \ \langle f'_i(^3A'') \rangle \ + \ \sigma(^3A') \ \langle f'_i(^3A') \rangle}{\sigma(^3A'') \ + \ \sigma(^3A')} \qquad (4)$$

From this equation, it can be seen that the total average fractions of energy are dominated by those of the barrierless ^{3}A'' ground PES, since $\sigma_l(^3A'')$ is generally much larger than $\sigma_l(^3A')$.

More detailed information on the energy distribution can be obtained from the vibrational populations of N_2. The QCT vibrational distributions from reaction (1) with NO(v=0-2,*j*=1,8,12) on both PESs at selected E_T values [0.0125 eV (^{3}A'') and 0.40 eV (^{3}A')] are shown in Figure 5. In all cases the distributions present population inversion and the ^{3}A'' surface leads to less vibrational excitation than the ^{3}A' surface, and the distributions are little dependent of collision energy and rotational state of NO (see also Ref.24). Vibrational inversion is expected for exothermic reactions and the larger vibrational excitation found in the ^{3}A' PES comes from the early barrier character of this surface. As indicated in the previous section, the cross sections for the production of N_2 in specific vibrational states from N + NO(*v*=0-2,*j*=1,8,12) are reported in Ref.24.

The influence of vibrational excitation of NO on the vibrational populations of N_2 is particularly important, differing from what happens for E_T and the NO rotational energy. In fact, the addition of one or two quanta of vibrational energy in NO leads to significant changes in the vibrational populations of N_2, even though the vibrational energy values involved (0.24 and 0.48 eV

above the energy of NO(v=0) for v=1 and 2, respectively) are small in comparison with the total available energy in products (3.4 and 3.8 eV for the ^{3}A'' and ^{3}A' PESs for NO(v=1), respectively, as different E_T values were considered in both surfaces). Moreover, the influence of NO vibrational excitation is more evident for the ground PES than for the excited one.

Due to the very low reactivity presented by reaction (2), only the global NO vibrational populations arising from N + N'O at T = 3000 and 5000 K have been determined here (see Ref. 24). The NO vibrational populations are not inverted [the NO(v'=0) level is clearly the most probable one], which strongly contrasts with the results observed for reaction (1) under the same thermal conditions.[24] This could be expected from the thermoneutral character of reaction (2), while reaction (1) is exothermic. In both reaction channels the distributions become wider as temperature increases, which implies that more vibrational and rotational levels become available.

D. Two- and three-vector correlations

Having completed the study of the scalar properties of the N + NO reactive system, we then examined the stereodynamics (vector properties) of reaction (1), taking into account relevant vectors of the system. We analyzed the two-vector angular distributions **kk'**, **kj'** and **k'j'** (where **k** and **k'** correspond to the initial and final relative velocity vectors, respectively, and **j'** refers to the rotational angular momentum vector of NO). The **kk'** angular distribution was expressed in terms of the differential cross section per unit of solid angle, $d^2\sigma/d\Omega$ (DCS hereafter), and using its dimensionless form ($2\pi/\sigma$ times the $d^2\sigma/d\Omega$ value; relative DCS hereafter), and the **kj'** and **k'j'** angular distributions were presented in terms of the probability density function [P(**kj'**) and P(**k'j'**), respectively].[26] Representative data of the **kk'**, **kj'** and **k'j'** distributions are given in Figures 6-8, and we also analyzed the three-vector angular distribution corresponding to the **kk'j'** dihedral angle given in terms of the probability density function P(**kk'j'**)[26] (Figure 9)**.**

Figure 6 shows the global **kk'** angular distribution for the ground and excited surfaces. Reaction (1) takes place with some tendency towards backward scattering, this being more evident as collision energy increases. The ^{3}A'' PES has a lower tendency towards backward scattering than the ^{3}A' PES, but the relative DCS(**kk'**) of both surfaces gradually tend to show a similar shape (backward preference) as collision energy increases. The differences observed between the ^{3}A'' and ^{3}A' surfaces can be interpreted on the basis of the absence and presence of a barrier on the minimum energy path, respectively. Moreover, The analysis of the opacity function [reaction probability ($P_r(b)$) vs. the initial impact parameter (b)] also helps to rationalize the behavior of the **kk'** angular distribution, in the case of reactions occurring through a direct reaction mode. Thus, the larger b_{max} values recorded for the ground PES in comparison with those for the excited PES suggest that the system will show a weaker trend towards backward scattering on the former surface, as it was really found in the calculations.

The **kj'** angular distributions for reaction (1) on the two PESs studied are symmetric around 90º, as they must be, due to the invariance of the distribution of the product molecule internuclear axis by reflection on the **kk'** plane.[26] At this angle, they exhibit a maximum and the behavior of P(**kj'**) of both surfaces is similar (Figure 7). This trend towards a perpendicular arrangement of the **k** and **j'** vectors can be rationalized on the basis of the transformation of angular momentum vectors when evolving from reactants into products, and is fairly typical of a direct reaction.

For the ^{3}A'' PES and the j=8 and 12 rotational levels of NO, P(**kj'**) evolves from a rather isotropic distribution at 0.0125 eV to a distribution with a maximum at 90º, which is already evident at 0.10 eV.[24] By the contrary, the evolution of the distribution for j=1 is not monotonic. The behavior of P(**kj'**) is simpler for the ^{3}A' PES, the distribution becoming for all j values a bit wider as collision energy increases. For both surfaces, there is no tendency for **j'** to be aligned along **k**, and the condition j=1 shows a somewhat larger tendency than conditions j=8 and 12 to lead to products with **j'** aligned perpendicular to **k**.

The **k'j'** angular distributions of reaction (1) on the PESs studied correspond to a symmetric distribution around 90º, as expected, due to the reflection symmetry in the scattering plane,[26] and are similar to the **kj'** distributions (Figure 8). These results correlate with the dependence exhibited by the **l'j'** angular distribution, where **l'** is the orbital angular momentum vector of products, which, although it cannot be determined experimentally, is helpful in interpreting the **k'j'** distribution results. In fact, the trend towards parallel or anti-parallel **l'j'** orientation observed in the calculations leads to a tendency towards a perpendicular **k'j'** orientation.

For the ^{3}A'' PES and all j values, P(**kj'**) evolves from a relatively narrow distribution, with a maximum at 90º for E_T=0.0125 eV, to a rather isotropic distribution at 0.20 eV, showing some preference for **j'** to be aligned parallel or antiparallel to **k'** at higher energies. The behavior of P(**kj'**) is similar for the ^{3}A' PES, although it has a tendency to show a maximum at 90º. This distribution is quite isotropic at the higher collision energies (0.8 and 1.0 eV), which is particularly evident for the v=1 and v=2 levels of NO.[24]

Up to now the results obtained suggest that the reaction mode of the N + NO → N_2 + O reaction is essentially direct, and this is corroborated by the P(**kk'j'**) data (Figure 9). The ϕ angle (or **kk'j'** angle) is the dihedral angle arising from the plane defined by vectors **k'** and **j'** with respect to that one defined by **k** and **k'**. The interest of this property was shown in the pioneering work of Herschbach and coworkers on statistical long-lived complex-forming reactions, where P(**kk'j'**) is symmetric around 180º (see, e.g., Ref. 27). Figure 9 shows that the rotational angular momentum vector of N_2 tends to rotate perpendicularly to the **kk'** plane (scattering plane), and this corresponds to the dihedral angles of 90º and 270º. For the ^{3}A'' PES there is a significant orientation of **j'** with respect to the scattering plane that decreases as collision energy increases, while for the ^{3}A' PES the preferred orientation evolves from ϕ=90º at the lower energies to ϕ=270º at the higher ones.[24]

Two- and three-vector properties for reaction (1) for other (E_T,v,j) initial conditions can be found in Ref.24. On the overall, the results are similar to the ones described here.

E. Microscopic reaction mechanism

The reaction mode was analyzed for reactions (1) and (2) on the ground and excited PESs at 1000, 3000 and 5000 K. To do this, we considered representative samples of reactive trajectories and analyzed the evolution of the three internuclear distances over time. The most important types of reactive trajectories observed are shown in Figure 10.

Reaction (1) on the ^{3}A" PES essentially occurs in a direct way (Fig. 10a) and only about 2 % of the reactive trajectories (3000-5000 K) lead to the formation of short lived collision complexes (Fig. 10b). When this reaction is considered on the ^{3}A' PES, the formation of collision complexes is far greater than for the ^{3}A" PES (54, 32 and 17 % for 1000, 3000, and 5000 K, respectively; see Figs. 10c and 10d).

Reaction (2) on the ^{3}A" PES mainly takes place in a direct way (54 and 71 % at 3000 and 5000 K, respectively), although an indirect migration mechanism, where the N atom first attacks the N' atom end of N'O molecule, is also important here (46 and 28 % at 3000 and 5000 K, respectively; see Figs. 10e and 10f). If this reaction occurs on the ^{3}A' PES, the percentage of reactive events occurring via a direct mechanism is reduced (25-58 % at 3000-5000 K), and an indirect reaction mode involving the formation of collision complexes makes a very significant contribution to the reactivity (74-37 % at 3000-5000 K; see Figs. 10g and 10h). The indirect migration mechanism is essentially negligible in the excited surface.

In general, the results obtained for reaction (1) can be interpreted according to the H-H-H (heavy-heavy-heavy) kinematics of the system, and taking into account that the ground PES is barrierless, while the excited PES has a significant barrier.[4] This allows the system to evolve more rapidly into products through the first PES.

For reaction (2), the formation of collision complexes on the ^{3}A' PES and the absence of this reaction mode on the ^{3}A'' PES can also be understood if we consider the shapes of the two PESs. In fact, the NON(^{3}A') minimum involved in the N-atom exchange process is energetically easier to reach from reactants (1.184 vs. 1.756 eV, along the corresponding MEP, for the ^{3}A' and ^{3}A" surfaces, respectively) and much deeper (0.585 vs. 0.0520 eV) than the NON(^{3}A") minimum.[4]

IV. Summary and conclusions

In this work we analyzed the kinetics of the N + NO → N_2 + O reaction, using the QCT method and two *ab initio* analytical surfaces developed by our group for the ground (^{3}A'' PES) and first excited (^{3}A' PES) states of this system. Moreover, the kinetics of the N + N'O → NO + N' has also been examined.

We also investigated the influence of collision energy and the rovibrational state of NO on a broad set of N + NO → N_2 + O dynamic properties (cross sections, product state distributions, angular distributions, and microscopic reaction mechanism).

Reaction (1) dominates the reactivity of the N + NO system over the T range and (E_T, v, j) conditions studied, as expected from the large energy barriers associated to reaction (2). On the other hand, the ground PES, which is barrierless for reaction (1), plays a dominant role, as the excited PES has a significant energy barrier along the MEP of this reaction.

The QCT results are generally in good agreement with the VTST and most of the RWP-J shifting results for both reactions and both PESs. They are also in good agreement with the experimental kinetics data for reaction (1), including the most recent low temperature data, and taking into account the experimental error margins. The dynamic results obtained as a function of (E_T, v, j) were rather easily interpreted according to the properties of the two PESs involved and the kinematics (H-H-H mass combination) of the system.

QCT calculations using the ground and first excited PESs developed in our group could also be very useful for the determination on new equilibrium and non-equilibrium (i.e, $T_{vib} \neq T_{trans} = T_{rot}$) reaction rates at very high temperatures (e.g., 5000-15000 K), which are necessary to model in a more accurate way hypersonic re-entry flows into the Earth's atmosphere.[28] This could be done for both N + NO → N_2 + O and its reverse reaction, using the same PESs.

Acknowledgements

This work was supported by the Spanish Ministry of Education and Science (Projects No. CTQ2005-09334-C02-01 and CTQ2006-02195) and by the Spanish Ministry of Science and Innovation (Projects No. CTQ2008-06805-C02-01 and CTQ2009-07647), and thanks are also given to the "Generalitat de Catalunya" (Autonomous Government of Catalonia, Grants No. 2005SGR 00175 and 2009SGR 17).

Tables

Table I. QCT, VTST and RWP-J shifting rate constants for reaction (1) on the $^3A''$ and $^3A'$ PESs (in $cm^3\ s^{-1}$).

T / K	QCT $k_I(^3A'')$	VTST[a] $k_I(^3A'')$	RWP[b] $k_I(^3A'')$	QCT $k_I(^3A')$	VTST[c] $k_I(^3A')$	VTST[d] $k_I(^3A')$	RWP[e] $k_I(^3A')$
10	2.35×10^{-11}		8.85×10^{-12}				
25	3.34×10^{-11}		2.04×10^{-11}				
40	3.72×10^{-11}		3.15×10^{-11}				
50	3.78×10^{-11}		3.59×10^{-11}				
100	3.38×10^{-11}		4.09×10^{-11}		5.55×10^{-31}	2.90×10^{-30}	
200	2.74×10^{-11}	6.51×10^{-11}	3.66×10^{-11}		1.57×10^{-21}	2.20×10^{-21}	5.90×10^{-18}
400	2.42×10^{-11}	3.78×10^{-11}	3.27×10^{-11}		9.34×10^{-17}	1.01×10^{-16}	3.49×10^{-17}
600	2.34×10^{-11}	3.19×10^{-11}	3.23×10^{-11}		4.14×10^{-15}	4.29×10^{-15}	1.26×10^{-15}
1000	2.41×10^{-11}	3.02×10^{-11}	3.39×10^{-11}	8.60×10^{-14}	1.02×10^{-13}	1.03×10^{-13}	3.50×10^{-14}
1500	2.57×10^{-11}	3.01×10^{-11}	3.67×10^{-11}	5.15×10^{-13}	5.85×10^{-13}	5.88×10^{-13}	2.11×10^{-13}
2000	2.79×10^{-11}	3.06×10^{-11}	3.89×10^{-11}	1.35×10^{-12}	1.52×10^{-12}	1.52×10^{-12}	5.17×10^{-13}
3000	3.18×10^{-11}	3.33×10^{-11}		3.86×10^{-12}	4.40×10^{-12}	4.41×10^{-12}	
4000	3.65×10^{-11}	3.67×10^{-11}		7.15×10^{-12}	8.09×10^{-12}	8.10×10^{-12}	
5000	4.05×10^{-11}	4.05×10^{-11}		1.10×10^{-11}	1.22×10^{-11}	1.22×10^{-11}	

[a] The ICVT-SO data were calculated but not reported in Ref. 4, and are identical to the ICVT/μOMT-SO results. For the $^3A''$ PES only VTST no scaled data were calculated in Ref. 4, because this surface has no energy barrier along the MEP of reaction (1).

[b] RWP-*J* shifting data for $T \geq 200$ K taken from Ref. 12.

[c] ICVT-SO no scaled data for the $^3A'$ PES (calculated but not reported in Ref. 4) .

[d] ICVT/μOMT-SO no scaled data for the $^3A'$ PES (calculated but not reported in Ref. 4).

[e] RWP-*J* shifting data from Ref.12.

Table II. QCT, VTST, RWP-*J* shifting and experimental total rate constants for reaction (1) ($k_1 \times 10^{11}$ in $cm^3\ s^{-1}$).

T / K	QCT	VTST[a]	RWP[a]	Experimental				
10	2.35		0.89					
25	3.34		2.04					
40	3.72		3.15					
50	3.78		3.59	5.9±2.8[b]				
100	3.38		4.09	4.3±1.4[b]				
200	2.74	6.51	3.66	3.7±1.0[b]	3.8±1.5[c]	3.5±2.0[d]	5.2±1.7[e]	
400	2.42	3.78	3.27		2.7±0.5[c]	"	3.3±0.7[e]	3.2±1.4[f]
600	2.34	3.19	3.23			"		4.4±1.6[f]
1000	2.42	3.04	3.39			"		
1500	2.62	3.11	3.69			"		
2000	2.92	3.29	3.94			"		
3000	3.57	3.77				"		
4000	4.37	4.48				"		
5000	5.14	5.27						

[a] VTST and RWP-*J* shifting data for $T \geq 200$ K taken from Ref.12.

[b] Exp. recommended values from Ref.23.

[c] Exp. values from Ref.21.

[d] Exp. recommended values from Ref.22. The same value applies for *T*: 200-4000 K.

[e] Exp. recommended values from Ref.20.

[f] Exp. values from Ref.19.

Table III. QCT and VTST rate constants for reaction (2) on the $^3A''$ and $^3A'$ PESs and total rate constant for this reaction (in $cm^3\ s^{-1}$).

T / K	QCT $k_2(^3A'')$	VTST[a] $k_2(^3A'')$	QCT $k_2(^3A')$	VTST[a] $k_2(^3A')$	QCT k_2	VTST k_2
1000		1.74×10^{-20}	7.72×10^{-18}	1.38×10^{-17}	7.72×10^{-18}	1.38×10^{-17}
1500		1.66×10^{-17}	3.55×10^{-16}	1.18×10^{-15}	3.55×10^{-16}	1.20×10^{-15}
2000		5.68×10^{-16}	4.45×10^{-15}	1.20×10^{-14}	4.45×10^{-15}	1.26×10^{-14}
2500	7.59×10^{-15}	5.00×10^{-15}	2.05×10^{-14}	5.09×10^{-14}	2.81×10^{-14}	5.59×10^{-14}
3000	2.92×10^{-14}	2.21×10^{-14}	7.71×10^{-14}	1.38×10^{-13}	1.06×10^{-13}	1.60×10^{-13}
4000	1.51×10^{-13}	1.51×10^{-13}	3.15×10^{-13}	5.13×10^{-13}	4.66×10^{-13}	6.64×10^{-13}
5000	5.68×10^{-13}	5.02×10^{-13}	7.94×10^{-13}	1.19×10^{-12}	1.36×10^{-12}	1.69×10^{-12}

[a] VTST results (ICVT method with SCT tunneling correction) from Ref. 4.

Figure captions

Figure 1. QCT (□), VTST[4,12] (○), and RWP-J shifting[12] (Δ) rate constants for reaction (1), as a function of temperature, on the ground ^{3}A'' (a) and excited ^{3}A' (b) PESs. The total rate constant (^{3}A''+^{3}A') and the Arrhenius plot (log k vs 1/T) for the ^{3}A'' PES are presented in (c) and (d), respectively. Some experimental values have also been added [data from Ref. 22 (⊙) in (c), and data from Ref. 20 (◈) and Ref 23 (⊙) in (d)]. The VTST and RWP-J shifting results below 100 K have been calculated here. See Tables I-II for details on the VTST level of calculations.[4]

Note: Figure 1 is suggested to be in color online

Figure 2. QCT (□) and VTST[4,12] (○) rate constants for reaction (2), as a function of temperature, on the ground ^{3}A'' (a) and excited ^{3}A' (b) PESs. The total rate constant (^{3}A''+^{3}A') is presented in (c). See Table III for details on the VTST level of calculations.[4]

Note: Figure 2 is suggested to be in color online

Figure 3. QCT cross sections for reaction (1) with NO(v=0,j) on the ground ^{3}A'' (a) and excited ^{3}A' (b) PESs, as a function of collision energy and for j=1 (■), j=8 (●), and j=12 (▲).

Note: Figure 3 is suggested to be in color online

Figure 4. QCT average energy fractions in products of reaction (1) with NO(v=0,j) on the ground ^{3}A'' (a) and excited ^{3}A' (b) PESs, as a function of collision energy and for j=1 (black), j=8 (red), and j=12 (green): Translation (squares; T), vibration (circles; V), and rotation (triangles; R).

Note: Figure 4 is suggested to be in color online

Figure 5. QCT N_2 vibrational state distributions for reaction (1) with NO(v=0-2,*j*) on the ground ^{3}A'' (a-c) and excited ^{3}A' (d-f) PESs at selected collision energies [0.0125 eV (^{3}A'') and 0.40 eV (^{3}A')] and for *j*=1 (■), *j*=8 (●), and *j*=12 (▲).

Note: Figure 5 is suggested to be in color online

Figure 6. QCT **kk'** angular distribution, $2\pi DCS/\sigma$, for reaction (1) with NO(v=0,*j*) on the ground ^{3}A'' (a-c) and excited ^{3}A' (d-f) PESs at several collision energies, as indicated in each subfigure, and for *j*=1 (■), *j*=8 (●), and *j*=12 (▲).

Note: Figure 6 is suggested to be in color

Figure 7. QCT **kj'** angular distribution, *P*(**kj'**), for reaction (1) with NO(v=0,*j*) on the ground ^{3}A'' (a-c) and excited ^{3}A' (d-f) PESs at several collision energies, as indicated in each subfigure, and for *j*=1 (■), *j*=8 (●), and *j*=12 (▲).

Note: Figure 7 is suggested to be in color

Figure 8. QCT **k'j'** angular distribution, *P*(**k'j'**), for reaction (1) with NO(v=0,*j*) on the ground ^{3}A'' (a-c) and excited ^{3}A' (d-f) PESs at several collision energies, as indicated in each subfigure, and for *j*=1 (■), *j*=8 (●), and *j*=12 (▲).

Note: Figure 8 is suggested to be in color

Figure 9. QCT **kk'j'** angular distribution, *P*(**kk'j'**), where ϕ corresponds to the dihedral angle, for reaction (1) with NO(v=0,*j*) on the ground ^{3}A'' (a-c) and excited ^{3}A' (d-f) PESs at several collision energies, as indicated in each subfigure, and for *j*=1 (■), *j*=8 (●), and *j*=12 (▲).

Note: Figure 9 is suggested to be in color

Figure 10. Representation of the types of reactive trajectories found in the N + N'O system: For reaction N + NO (v,j) → N_2 + O on the ground PES [direct (a) and non direct (b) reaction mode] and on the excited PES [short lived collision complex formation (c, d)]; for reaction N + N'O (v,j) → N' + N'O on the ground PES [(e) and (f) show the migration of the N atom from the N' end to the O end of N'O] and on the excited PES [(g) and (h) show the formation of long lived collision complexes]. Distances are indicated as follows: R(N-N') green line, R(N'-O) black line and R(N-O) red line.

Note: Figure 10 is suggested to be in color

Figure 1.

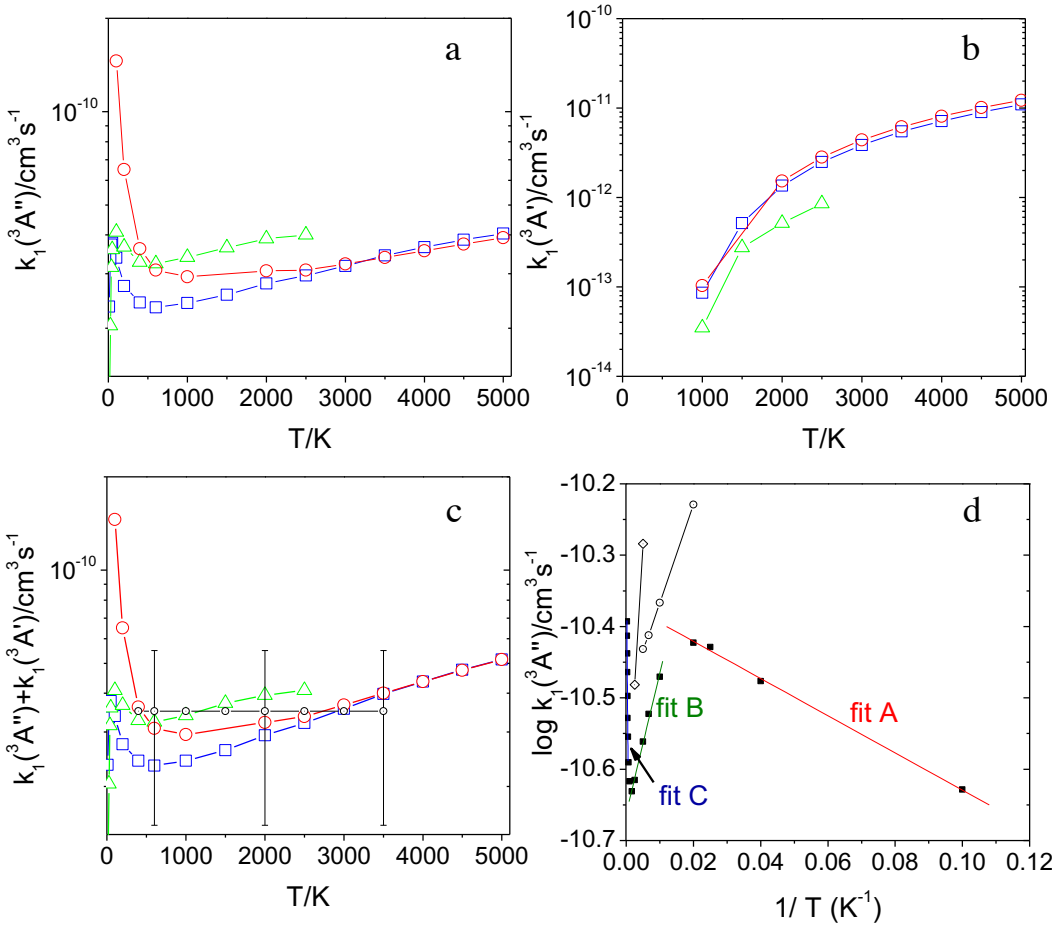

Figure 2.

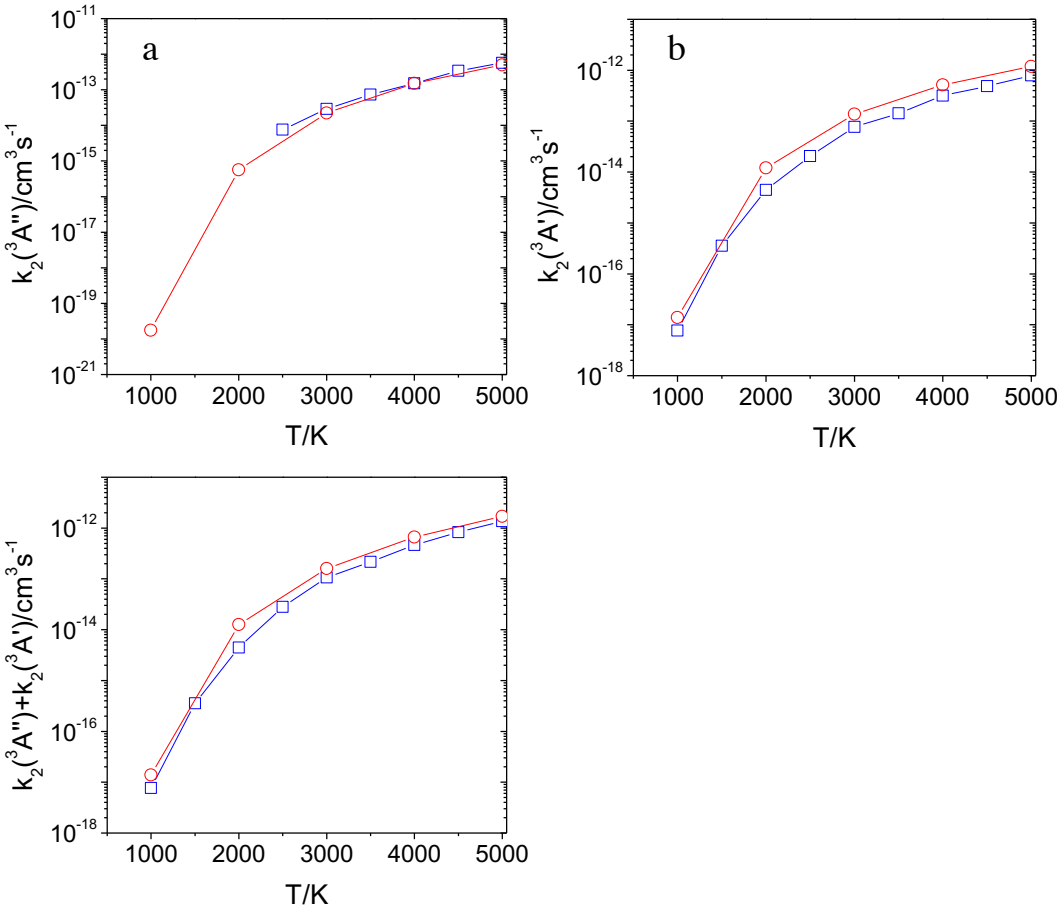
a
b
$k_2(^3A'')/cm^3s^{-1}$
$k_2(^3A')/cm^3s^{-1}$
$k_2(^3A'')+k_2(^3A')/cm^3s^{-1}$
T/K
1000
2000
3000
4000
5000

Figure 3.

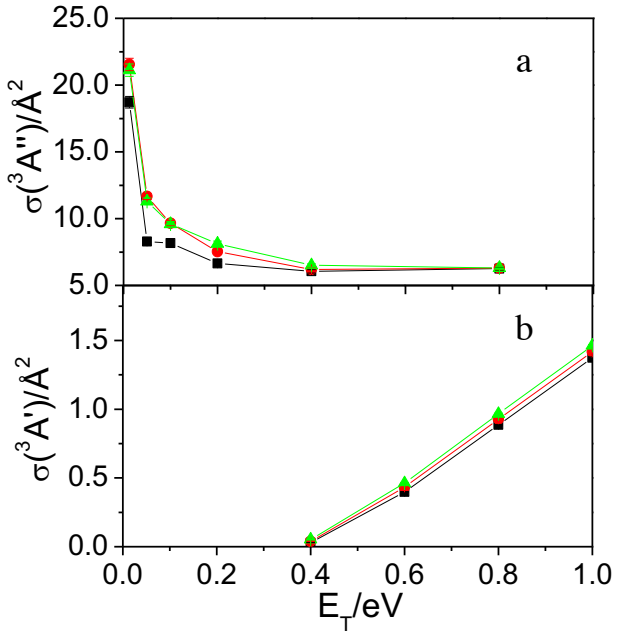
a
b
σ(3A'')/Å2
σ(3A')/Å2
25.0
20.0
15.0
10.0
5.0
1.5
1.0
0.5
0.0
0.0
0.2
0.4
0.6
0.8
1.0
ET/eV

Figure 4.

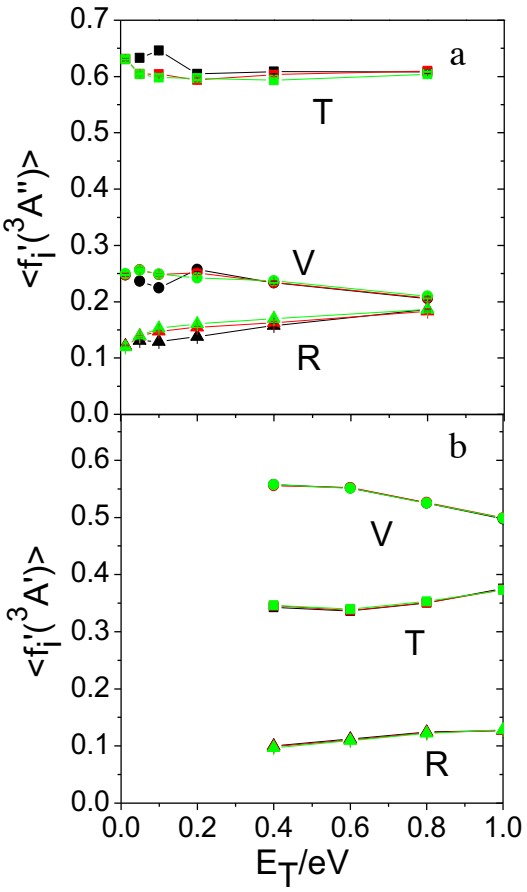

Figure 5.

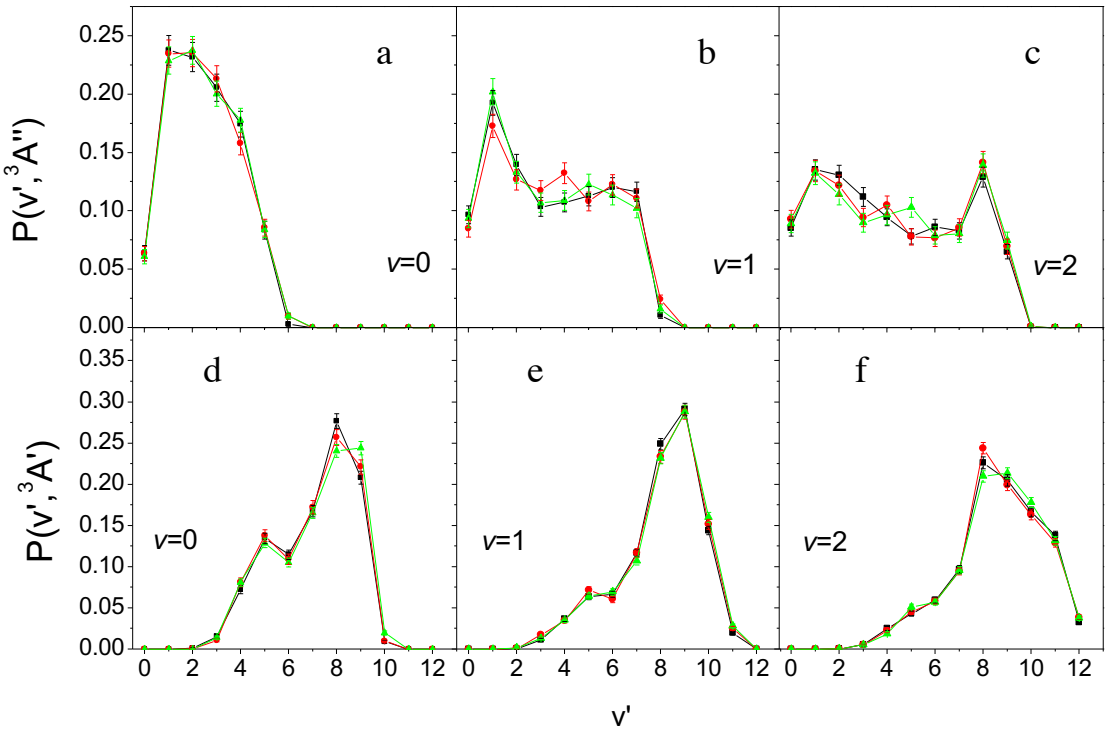
a
b
c
d
e
f
v=0
v=1
v=2
v=0
v=1
v=2
P(v',^{3}A'')
P(v',^{3}A')
v'
0.25
0.20
0.15
0.10
0.05
0.00
0.35
0.30
0.25
0.20
0.15
0.10
0.05
0.00
0 2 4 6 8 10 12

Figure 6.

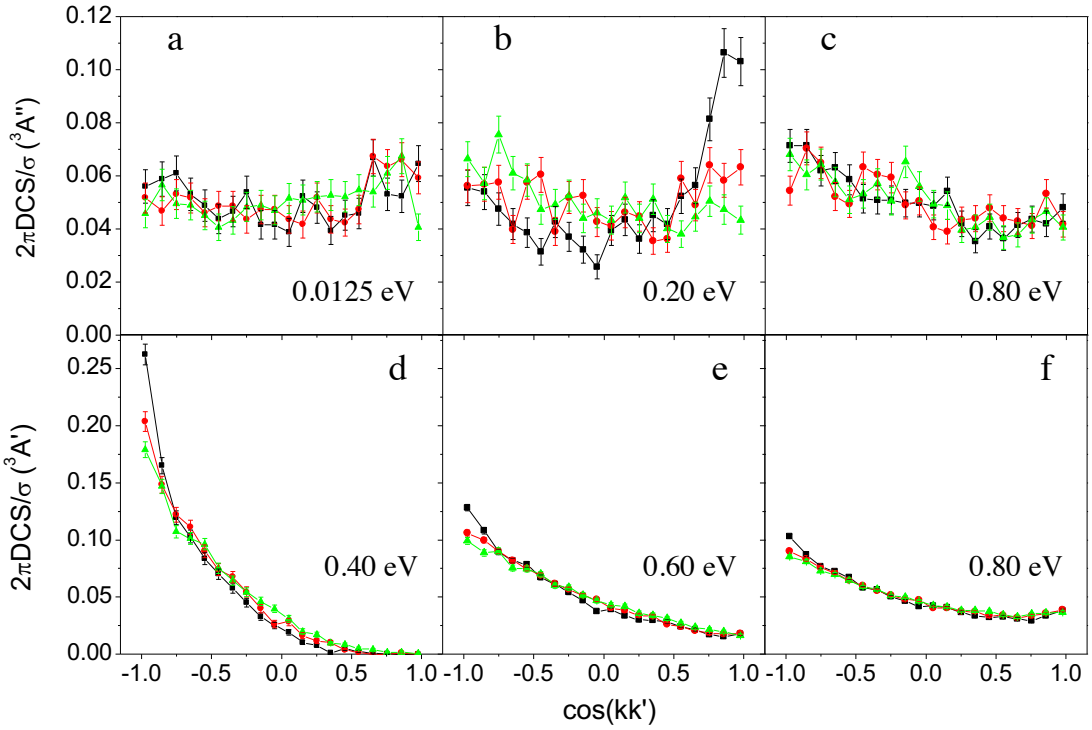
a
b
c
d
e
f
0.0125 eV
0.20 eV
0.80 eV
0.40 eV
0.60 eV
0.80 eV
2πDCS/σ (³A'')
2πDCS/σ (³A')
cos(kk')
0.12
0.10
0.08
0.06
0.04
0.02
0.00
0.25
0.20
0.15
0.10
0.05
0.00
-1.0
-0.5
0.0
0.5
1.0

Figure 7.

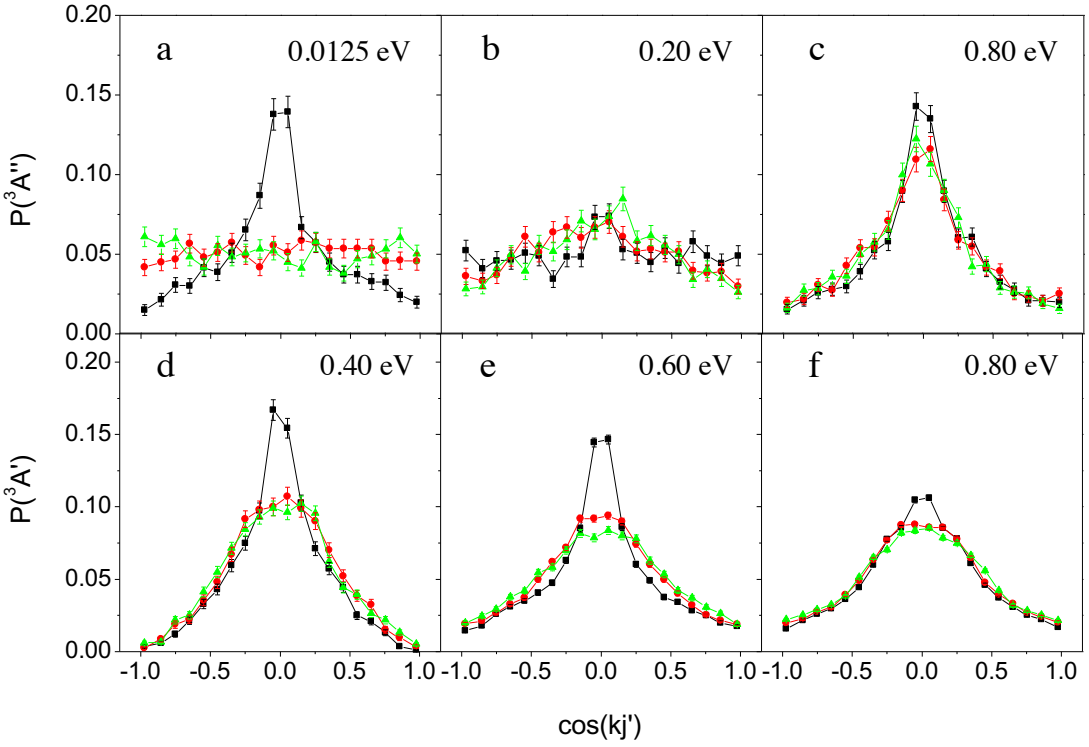
a
0.0125 eV
b
0.20 eV
c
0.80 eV
d
0.40 eV
e
0.60 eV
f
0.80 eV
P(3A'')
P(3A')
cos(kj')
0.00
0.05
0.10
0.15
0.20
-1.0
-0.5
0.0
0.5
1.0

Figure 8.

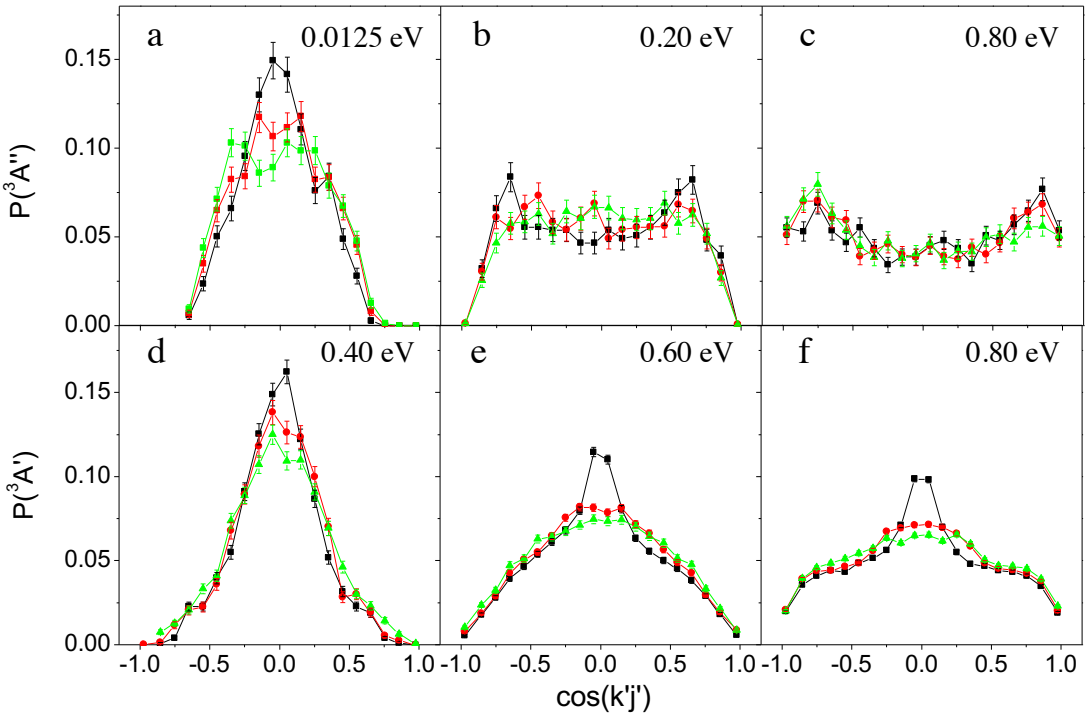
a
0.0125 eV
b
0.20 eV
c
0.80 eV
d
0.40 eV
e
0.60 eV
f
0.80 eV
P(3A'')
P(3A')
0.00
0.05
0.10
0.15
-1.0
-0.5
0.0
0.5
1.0
cos(k'j')

Figure 9.

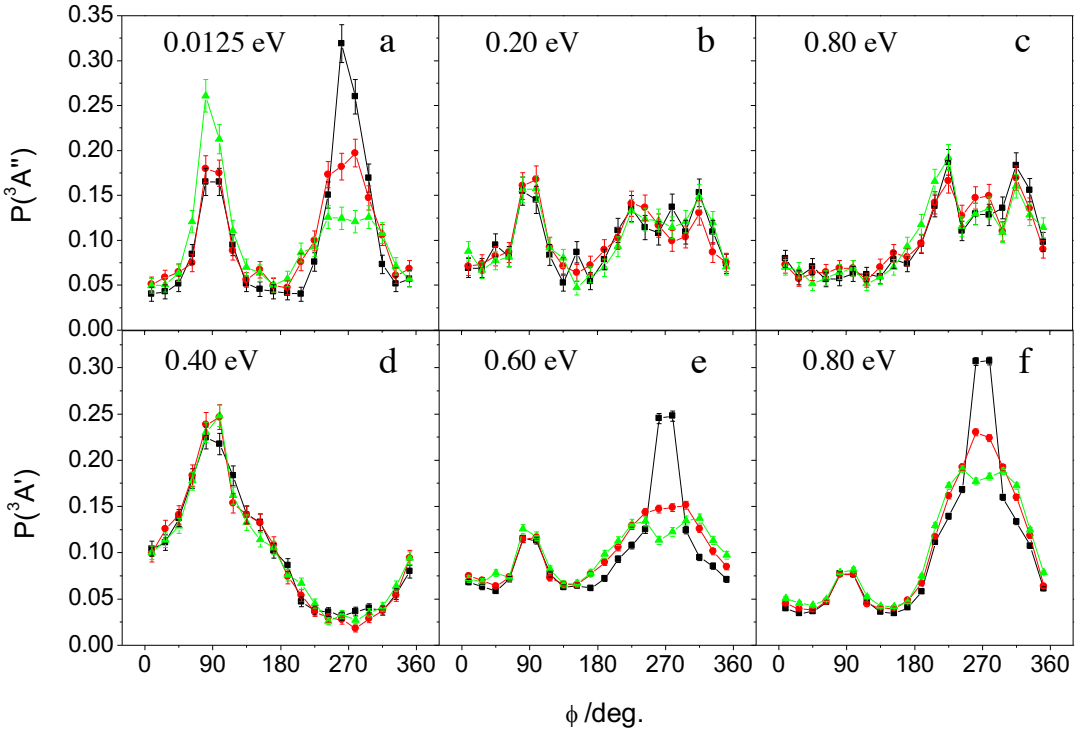
0.0125 eV
a
0.20 eV
b
0.80 eV
c
0.40 eV
d
0.60 eV
e
0.80 eV
f
P(3A'')
P(3A')
0.35
0.30
0.25
0.20
0.15
0.10
0.05
0.00
0
90
180
270
360
ϕ /deg.

Figure 10.

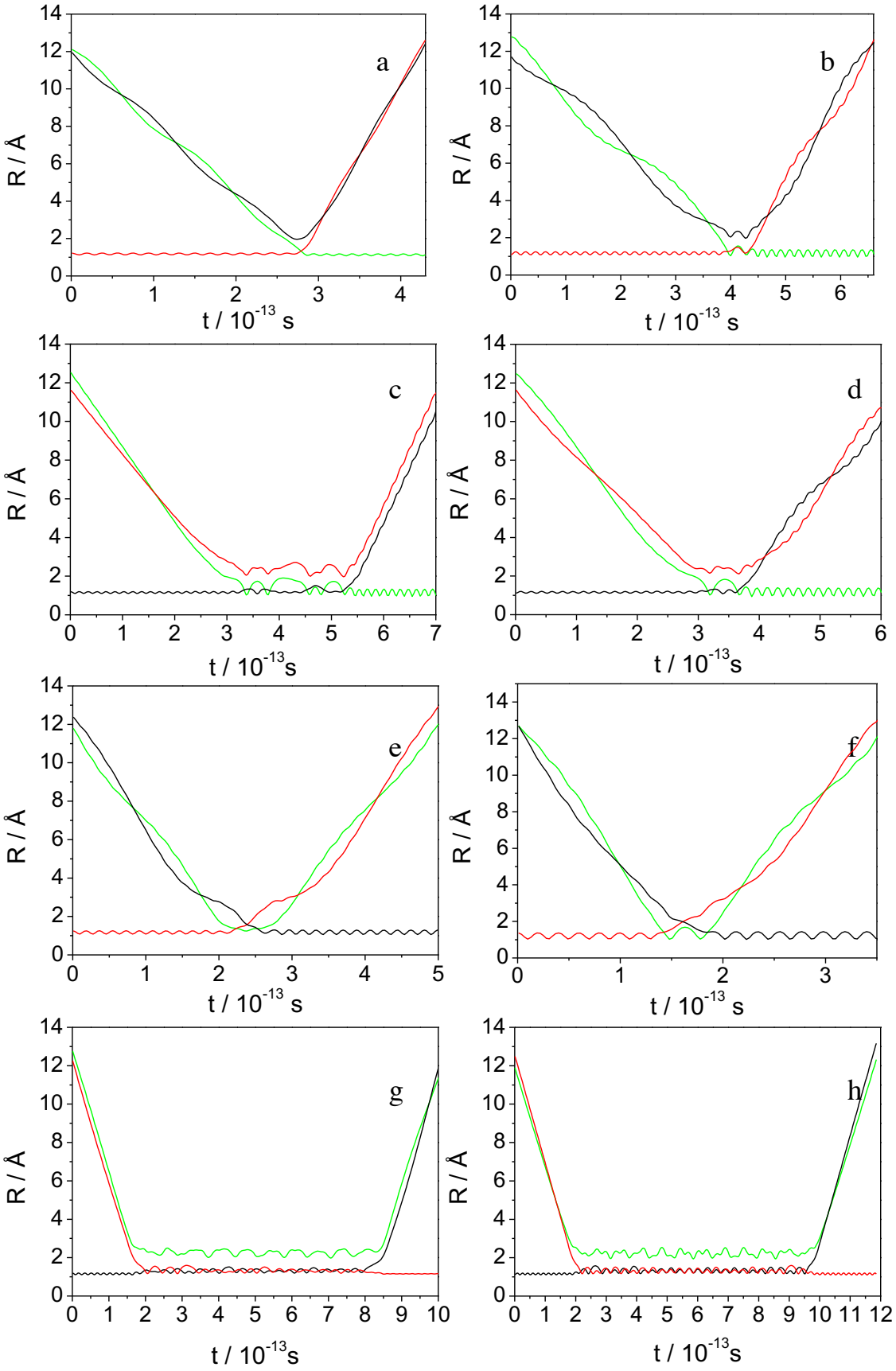

References

[1] M. W. Chase, Jr., C. A. Davies, J. R. Downey, Jr., D. J. Frurip, R. A. Mc. Donald, and A. N. Syverud, J. Phys. Chem. Ref. Data Suppl. **14**, 1 (1985).

[2] D. F. Strobel, J. Geophys. Res. **76**, 8384 (1971).

[3] G. Brassens and M. Nicolet, Planet. Space Sci. **21**, 939 (1973).

[4] P. Gamallo, M. González, and R. Sayós, J. Chem. Phys. **119**, 2545 (2003).

[5] J. Dubrin, C. Mackay, and R. Wolfgang, J. Chem. Phys. **44**, 2208 (1966).

[6] R. Iwata, A. Ferrieri, and A. P. Wolf, J. Phys. Chem. **90**, 6722 (1986).

[7] M. Gilibert, A. Aguilar, M. González, F. Mota, and R. Sayós, J. Chem. Phys. **97**, 5542 (1992).

[8] M. Gilibert, A. Aguilar, M. González, and R. Sayós, J. Chem. Phys. **99**, 1719 (1993).

[9] R. Sayós, A. Aguilar, M. Gilibert, and M. González, J. Chem. Soc. Faraday Trans. **89**, 3223 (1993).

[10] A. Aguilar, M. Gilibert, X. Giménez, M. González, and R. Sayós, J. Chem. Phys. **103**, 4496 (1995).

[11] P. Gamallo, M. González, R. Sayós, and C. Petrongolo, J. Chem. Phys. **119**, 7156 (2003).

[12] P. Gamallo, R. Sayós, M. González, C. Petrongolo, and P. Defazio, J. Chem. Phys. **124**, 174303 (2006).

[13] J. N. Murrell, S. Carter, S. C. Farantos, P. Huxley and A. J. C. Varandas, Molecular Potential Energy Surfaces (Wiley, New York, 1984).

[14] P. Gamallo, M. González, and R. Sayós, J. Chem. Phys. **118**, 10602 (2003).

[15] L. M. Raff and D. L. Thompson, in *Theory of Chemical Reaction Dynamics*, edited by M. Baer (CRC, Boca Raton, 1985) Vol. III.

[16] H. R. Mayne, Int. Rev. Phys. Chem. **10**, 107 (1991).

[17] I. Miquel, J. Hernando, R. Sayós, and M. González, J. Chem. Phys. **119**, 10040 (2003).

[18] R. Martínez, J. D. Sierra, and M. González, J. Chem. Phys. **123**, 174312 (2005).

[19] M. A. A. Clyne and I. S. McDermid, J. Chem. Soc. Faraday Trans. **71**, 2189 (1975).

[20] P. O. Wennberg, J. G. Anderson and D. K. Weisenstein, J. Geophys. Res. **99**, 18839 (1994).

[21] W. B. DeMore, S. P. Sander, C. J. Howard, A. R. Ravinshankara, D. M. Golden, C. E. Kolb, R. F. Hampson, M. J. Kurylo, M. J. Molina, *Chemical Kinetics and Photochemical Data for Use in Stratospheric Modeling*, Evaluation 12, NASA-JPL, Publication 97-4 (Pasadena, CA, 1997).

[22] D. L. Baulch, C. T. Bowman, C. J. Cobos, R. A. Cox *et al.*, J. Phys. Chem. Ref. Data **34**, 757 (2005).

[23] A. Bergeat, K. M. Hickson, N. Daugey, P. Caubet, and M. Costes, Phys. Chem. Chem. Phys **11**, 8149 (2009).

[24] See EPAPS Document No. _____ for the dynamics results obtained for all the reaction conditions investigated for the N + NO reaction. This document can be reached through a direct link in the online article's HTML reference section or via the EPAPS home page (http://www.aip.org/pubservs/epaps.html).

[25] G. Black, R. L. Sharpless and T. G. Slanger, J. Chem. Phys. **58**, 4792 (1973).

[26] F. J. Aoiz, M. Brouard, and P. A. Enriquez, J. Chem. Phys. **105**, 4964 (1996).

[27] S. K. Kim and D. R. Herschbach, Faraday Discuss. Chem. Soc. **84**, 159 (1987).

[28] M. A. Gallis, R. B. Bond, and J. R. Torczynski, J. Chem. Phys. **131**, 124311 (2009).